An Electrospray Ionization Source for Thermochemical Investigation with the Guided Ion Beam Mass Spectrometer

R. M. Moision and P. B. Armentrout
Department of Chemistry, University of Utah, Salt Lake City, Utah, USA

An electrospray ionization (ESI) source developed for use with the guided ion beam tandem mass spectrometer (GIBMS) is described. For accurate determination of thermochemistry using threshold collision-induced dissociation (TCID), it is essential that any source produces ions with four exacting characteristics: (1) high intensity, (2) stable signal, and well-defined energies both (3) kinetic, and (4) internal. To accomplish these objectives, the ions generated by the electrospray are collected using a radio frequency electrodynamic ion funnel and are then transferred into a hexapole ion guide where they are thermalized and subsequently passed into higher-vacuum regions for analysis. The resulting ion intensities using this source can exceed 10^6 ions/s. Stable beams (<10% variation in signal) can be generated over multiple hours. The kinetic energy distribution of ions emerging from this source has been shown to be well described by a Gaussian distribution with a full width half maximum (FWHM) of about 0.1–0.2 eV in the laboratory frame of reference. Finally, TCID results for ions generated with this source show excellent agreement with previously reported threshold values for ions generated using a variety of sources and experimental methodologies. This confirms that internal energies of the ions are well described by a Maxwell–Boltzmann distribution at room temperature. (J Am Soc Mass Spectrom 2007, 18, 1124–1134) © 2007 American Society for Mass Spectrometry

Since its introduction in the 1980s [1], electrospray ionization (ESI) has become a widely used source for mass spectrometry. The popularity of the ESI can be credited to a number of factors. In addition to its ability to gently transfer large biological molecules into the gas phase in multiple charge states, ESI sources benefit from being simple in design and robust in use. However, despite its widespread acceptance, the ESI source has been used in only a limited number of experiments for quantitative determination of thermochemical information [2–6]. This is unfortunate, given the ability of the ESI to easily produce a large number of interesting gas-phase biological ions [7–9], charged transition metals [10–12], and alkali metal/ligand complexes [12–14]. The scarcity of thermochemical data originating from the ESI most likely lies in the difficulty of producing an ion beam that is suitable for rigorous thermochemical analysis. These prior ESI studies [2–6], where simpler ESI sources have been used to generate ions, have not thoroughly demonstrated whether such conditions (outlined below) have been reached.

Threshold collision-induced dissociation (TCID) experiments represent a well-established means of obtaining accurate thermochemical data for a diverse range of gas-phase ions [15–20]. Essentially, TCID consists of systematically varying the kinetic energy of a mass selected ion beam and then colliding the ions with a stationary non-reactive gas such as xenon. With increasing collision energy, the parent ion begins to fragment into products that are then collected as a function of the collision energy. The resulting data may be modeled to determine the absolute minimum, or threshold, energy necessary for each fragmentation pathway. Clearly, to rigorously quantify the threshold energy required for fragmentation, the kinetic and internal energy of the ions—*before* collision with the stationary gas—must be known.

One of the challenges in the development of a source suitable for TCID experiments is that it must produce ions with well-defined internal and kinetic energies in addition to the more conventional requirements of any source, good stability, and high intensity. Importantly, once the ions are created, the ion beam must be characterized to verify that the kinetic and internal energy distributions are well defined. In the vast majority of mass spectrometry applications using an ESI, one or possibly two of these demands might be required of the source, but rarely must an ESI source simultaneously satisfy all of these considerations. Here we describe the development of an ESI source suitable for quantitative threshold determination using the GIBMS.

Address reprint requests to Prof. Peter B. Armentrout, University of Utah, Department of Chemistry, 315 S 1400 E, Room 2020, Salt Lake City, UT 84112. E-mail: armentrout@chem.utah.edu

1044-0305/07/$32.00
doi:10.1016/j.jasms.2007.03.011

Published online April 26, 2007
Received February 6, 2007
Revised March 21, 2007
Accepted March 22, 2007

Experimental

The GIBMS

The guided ion beam mass spectrometer (GIBMS) instrument, data collection, and subsequent data analysis have been described in detail on a number of previous occasions and will be only briefly described here [15, 16, 19, 21]. Ions produced in the source region are initially mass selected in a magnetic momentum analyzer. The mass selected ions are decelerated to a well-defined kinetic energy and are focused into a radio frequency (rf) octopole ion guide that traps the ions radially [22, 23]. For TCID experiments, the octopole passes through a static gas cell containing xenon. After passing through the collision cell, any product ions and the remaining reactant ions drift to the end of the rf octopole where they are mass analyzed using a quadrupole mass filter and processed using standard counting techniques.

Ion intensities, measured as a function of collision energy, are converted to absolute cross sections using a Beer's Law relationship [21]. The absolute zero of energy for the ion beam is determined using a retarding potential technique by systematically varying the DC voltage on the octopole. The derivative of the onset energy is fit to a Gaussian distribution with the center of the fit defining the zero of kinetic energy (KE_0) of the ion beam and the full width at half maximum (FWHM) of the distribution describes the kinetic energy spread. Ion kinetic energies in the laboratory frame (Lab) are converted to energies in the center-of-mass (CM) frame using $E_{CM} = E_{Lab}m/(m + M)$, where M and m are the masses of the ionic and neutral reactants, respectively.

Most data presented herein are compared to a DC discharge/flow tube source (DC/FT) which has been used for a large number of studies in this laboratory [16–19, 24] and others [25–27]. The DC/FT source has been well described and has produced thermochemistry for a vast array of systems that is consistent with other experimental methodologies as well as ab initio calculations. Thermalization of the ions' internal modes in the DC/FT is accomplished by roughly 10^5 collisions between the ions and the helium bath gas as they pass through a nearly 140-cm-long flow tube at room temperature (~300 K). This results in the ions acquiring internal energies (rotational and vibrational) that are well described by a Maxwell–Boltzmann distribution at 300 K. One of the limitations of the DC/FT is that solid samples (e.g., amino acids) must be introduced into the gas phase by gentle heating. For many of these samples, the temperatures required to generate sufficient vapor pressure of the solid necessary to produce a high intensity ion beam often result in decomposition of the molecule being favored over vaporization. This effect either limits the intensity of the resultant ion beam of interest or can lead to non-thermalized ions or ions of different structure than anticipated.

Thermochemical Analysis

Modeling of the threshold regions of the CID reaction cross sections using the GIBMS have been described previously [20, 21, 28]. In short, the cross sections are modeled using the following equation:

$$\sigma(E) = \sigma_0 \sum_i g_i (E + E_i - E_0)^n / E \quad (1)$$

where σ_0 is an energy-independent scaling factor, n is an adjustable parameter that characterizes the efficiency of collisional energy deposition [20], E is the relative kinetic energy of the reactants in the center of mass frame, and E_0 is the threshold for CID of the ground electronic and rovibrational state of the reactant ion. The summation is over the rovibrational states of the reactant ions i, where E_i is the excitation energy of each state and g_i is the fractional population of those states ($\sum g_i = 1$). Before comparison with experimental data, eq 1 is convoluted to account for the kinetic energy of the reactant ion and thermal broadening of the neutral gas [29, 30].

Multiple reactant ion/neutral collisions can systematically obscure the interpretation of data resulting in extracted threshold energies being inaccurately low. For this reason, the pressure of xenon in the collision cell is deliberately kept low (0.04–0.12 mTorr). In this range of pressures, the probability of an ion undergoing a *single* collision is roughly 4–10%. Therefore, the majority of parent ions (>90%) pass through the collision cell without any interaction with the neutral gas. All data are collected at multiple collision pressures (usually 0.04, 0.08, and 0.12 mTorr) and the resulting cross sections are extrapolated to 0 mTorr, giving rigorous single collision conditions for analysis.

A further consequence of the requirement for low collision cell pressures is that the intensities of product channels with small reaction probabilities can be close to or below the signal-to-noise ratio of the instrument. Because these lesser reaction channels often provide the most interesting information about a TCID reaction, it is of great value to have a parent ion beam with the greatest possible intensity. With a parent ion beam of 10^5 ions/s and collision gas pressure of 0.10 mTorr, a cross section of 0.1×10^{-16} cm^2 is produced from a product ion intensity of 25 ions/s, close to the sensitivity level of the GIBMS. Therefore, a reactant ion beam intensity of about 10^5 ions/s is sufficient for collecting accurate information on the majority of product channels and intensities of 10^4 ions/s allow major products to be scrutinized carefully.

For the ions that do undergo a collision, the energy imparted is efficiently randomized into internal modes, making dissociation increasingly inefficient for larger molecules. As a result, post-collisional ions with internal energies above the threshold energy may not dissociate during the timescale of the experiment, about 5×10^{-4} s. This results in an observed threshold with an onset delayed by a kinetic shift that increases as the size

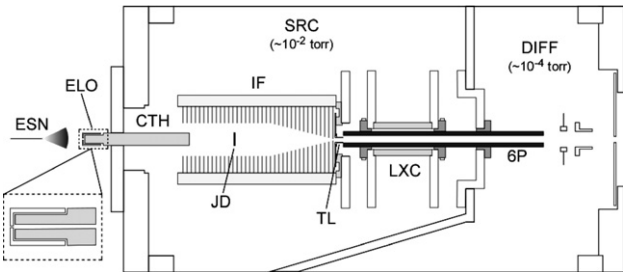

Figure 1. Schematic diagram of the electrospray ionization source designed for the guided ion beam tandem mass spectrometer (GIBMS). The electrospray needle (ESN), consisting of 35-gauge stainless steel tubing. ESI ions are transferred into the first vacuum region, SRC (~10^{-2} Torr), through 0.030-in.-ID capillary tubing held in place by the capillary tubing holder (CTH). Ions are collected by the ion funnel (IF) and transferred into a hexapole (6P) by a tube lens (TL). The 6P passes through the ligand exchange cell (LXC) before entering the first differentially pumped region (DIFF; ~10^{-4} Torr). Large vertical plates shown are used to support the lens train on three rods (not shown).

of the molecule becomes larger. Rice–Ramsperger–Kassel–Marcus (RRKM) statistical theory is incorporated into eq 1 to estimate these kinetic shifts [31]. For the $H_3O^+(H_2O)_n$ clusters discussed below, these kinetic shifts are small (0.01–0.06 eV). For the larger Na^+(proline) system, which contains more vibrational modes and has a higher threshold, the shifts are slightly larger (~0.15 eV).

Electrospray Ionization Source

A schematic overview of the electrospray ionization/ion funnel/hexapole (ESI/IF/6P) source appears in Figure 1. Solutions containing the ions of interest are prepared at concentrations of 10^{-4}–10^{-5} M [e.g., 10^{-5} M proline + 10^{-5} M NaCl for Na^+(proline)]. Solutions are introduced using a syringe pump (Model 55-1111; Harvard Apparatus, Holliston, MA, USA) at flow rates of 0.01–0.10 mL/h (170–1700 nL/min). Electrospray needles (ESN) are prepared from 35-gauge, regular-wall, hypodermic stainless steel tubing (Small Parts, Miami Lakes, FL, USA). The needles are biased at 1300–2100 V relative to ground. The entire needle assembly is mounted on an XYZ translation stage that allows for fine-tuning of the location of the needle relative to the vacuum entrance orifice.

Ions emanating from the spray are transferred into the vacuum region by a short length (~4.0-in.) of 0.063-in. (1/16-in.) OD stainless steel capillary tubing. Such tubing is readily available from a number of HPLC suppliers and comes with standard ID values ranging from 0.010- to 0.040-in. ID Tubing of 0.030 in. ID is used in experiments described here. The 0.063-in./capillary tubing is held within a capillary tubing holder (CTH). The CTH is machined from 0.375-in.-OD/0.063-in.-ID tubing (High Pressure Equipment Company, Erie, PA, USA), which is reamed out to an ID of 0.067 in. to allow for insertion of the 0.063-in.-OD stainless steel capillary tubing. This design allows for different lengths and ID values of capillary tubing to be used and for the tubing to be changed without the need to vent the entire instrument.

The CTH is centered and electrically isolated using fittings made of PEEK thermoplastic. This permits the entire capillary to be biased independently and heated to >200 °C if necessary. The temperature of the CTH assembly is controlled using heating tape and a temperature controller (Model T16; Red Lion Controls, York, PA, USA) and the temperature monitored using a thermocouple. In normal operation, the temperature of the capillary is 50–150 °C and the entire assembly is generally biased at 25–50 V relative to ground.

The entrance to the 0.063-in.-OD capillary tubing is further restricted using an entrance limiting orifice (ELO) that is machined into a cap that slides over the entrance end of the CTH (which is machined to an OD of 0.250 in. to secure and center the cap). The ELO cap is machined from 0.375-in.-OD stainless steel rod that is reamed to an ID of 0.251 in. to a depth that leaves an end wall thickness of about 0.040 in. A small-diameter hole (0.006–0.015 in.) is drilled through the center such that this hole is centered with respect to the 0.063-in.-OD capillary tubing when the ELO is in place on the CTH. For capillary tubing IDs from 0.020 to 0.040 in., we have tested ELOs ranging in size from 0.006 to 0.020 in. and have found that when the diameter of the entrance hole is less than one half of the ID of the capillary tubing, the signal stability is greatly improved. Even with the smallest-diameter hole (0.006 in.) used to date, we have observed this enhanced stability without any loss of signal intensity. The ELO serves to throttle the gas load into the vacuum such that the diameter of the ELO is directly correlated to the pressure in the source region. We believe that the ELO also functions to hydrodynamically focus the gas into the center of the capillary tubing.

The lens train within the source region (SRC) is supported and centered using three 0.250-in. centerless ground stainless steel rods on a 3.50-in. BC. The rods are centered with respect to the vacuum chamber on both ends. This allows all of the components on the lens train to be centered radially within 0.004 in. with respect to each other. These support rods have been removed from Figure 1 for clarity. The SRC region of the instrument is pumped by a 300 L/s roots blower (Model EH 1200; Edwards High Vacuum, Sussex, UK) backed by a mechanical pump (Edwards model E2M175). The lens train continues into a differentially pumped region (DIFF). This region is pumped by an 1800 L/s diffusion pump (Model VHS-6; Varian, Inc., Palo Alto, CA, USA) backed by a mechanical pump (Varian model SD-451).

Ion Funnel

The ion funnel (IF) is based largely on the design of Smith et al. [32, 33]. Briefly, the ion funnel consists of a stack of electrically isolated ring electrodes (or plates)

with decreasing inner diameters in the direction of the exit. Each plate receives a signal consisting of a combination of rf and DC voltages. Equal and opposite phases of the rf signal are applied to adjacent plates. This oscillating field on the plates in conjunction with the physically tapering lenses focuses the ions radially into the center of the ion funnel. The out-of-phase rf signals oscillate symmetrically about a DC potential applied to each plate. From entrance to exit, the plates receive a linearly decreasing DC voltage. This DC voltage gradient helps to "pull" positively charged ions through the ion funnel. The combination of electric fields and physical geometry has been shown to give transmission efficiencies nearing unity at pressures up to 10 Torr [34]. This makes the ion funnel an ideal candidate for accepting the rapidly diverging ions emanating from an ESI capillary.

The plates for the ion funnel are machined from 0.020-in.-thick brass sheets into 1.625 × 1.625-in. squares with small tabs (0.1 × 0.1-in.) centered on two sides to allow for convenient electrical connections. These tabs are similar in size to the Smith design, although they are not used with their custom-made zero-insertion-force (ZIF) sockets. Rather, each plate is soldered to a 1-in. length of 28-gauge prestripped wire-wrap wire. The wires are then individually connected to the circuit board described below. This results in a rather tedious initial setup, but produces robust connections and allows for multiple configurations of ion funnel to be quickly assembled and tested. Each plate is electrically and physically separated from its neighbors using 0.020-in.-thick Teflon® sheet cut into 1.625 × 1.625-in. squares with an ID of 1.125 in. For the brass plates, the ID of the first 44 plates was held at 1.00 in. and the final 44 plates formed a linear taper from 1.00 in. to a final ID of 0.094 in. To align the plates relative to the ion funnel central axis, all plates and Teflon® spacers have four 0.252-in. holes on a 1.625-in. radius. The stack of brass plates and Teflon® spacers are then assembled onto four 0.250-in. ceramic tubes. For mounting and compressing the IF, lengths of 4-40 threaded rod pass through the four ceramic tubes. The threaded rods are fastened to a mounting plate that is secured and centered using the main support rods.

In total, 88 lenses are used in the ion funnel, making the overall length just under 4 in. Approximately 1 in. from the ion funnel inlet is an electrically isolated 0.25-in.-diameter metal disc or jet disrupter (JD) [35, 36]. This disc helps to prevent large solvent clusters from depositing further downstream on the hexapole (6P) and does not lead to a decrease in signal intensity for the mass range of ions investigated to date. Such deposits on the 6P can lead to electrostatic barriers being formed, which result in ion trapping and ultimately poorly defined kinetic energies and non-thermal internal energy distributions.

As mentioned earlier, each plate requires a combined rf and DC signal. We have designed our own custom circuit board using an inexpensive internet vendor (www.ExpressPCB.com). A single circuit board contains both rf and DC circuits, thus requiring only one electrical connection per plate (1/2 that of the Smith design). Surface-mount resistors (200 kOhm, 1/8 Watt, Size 1206, Allied Electronics, Fort Worth, TX, USA) and capacitors (0.01 μF, 100 V, Size 1206, Allied Electronics) are used on the board. The linear voltage gradient across the plates is defined by DC voltages on the entrance (DC^+) and exit (DC^-) ends of the resistor chain. General ion funnel conditions are $DC^+ = 15$ V (ion funnel entrance or upstream voltage) and $DC^- = 5$ V. The voltage on the jet disrupter is independently adjusted and typically gives optimum signal when it is close to that of DC^+. Therefore its voltage must be optimized each time the DC^+ or DC^- values are adjusted. The rf voltage is about 25 V peak to peak (Vpp) at a frequency of 1.2 MHz.

The rf signal is applied to the ion funnel using a sine-wave output from a signal generator (Model 33120A; Hewlett–Packard, Palo Alto, CA, USA) and is amplified with an rf amplifier (Model 2100L; ENI, Rochester, NY, USA). The signal from the amplifier is split into equal and opposite phases with a 50-ohm trifilar-wound ferrite-core balun transformer. The balun consists of two stacked FT-290 toroids (Amidon Associates, Costa Mesa, CA, USA) wrapped with 14-gauge magnet wire. We have found that the opposite phase signals generated when the balun is wrapped as a trifilar are more equally balanced relative to a bifilar design. This circuit is capable of driving an 88-plate ion funnel at roughly 50 Vpp at 1 MHz and 20 Vpp at 2 MHz.

A DC tube lens (TL) is placed at the interface between the ion funnel and hexapole. The tube lens is created from a modified IF plate having a central hole with an ID of 0.14 in. onto which a tube having an OD of 0.17 in. and a length of 0.15 in. is attached. It is physically separated from the final ion funnel plate using a single Teflon® spacer described earlier. The lens is inserted 0.05–0.10 in. into the 6P and is biased between the DC^- voltage of the ion funnel and the 6P bias (0 V). At the operating pressures in the ion funnel, this lens has little focusing effect on the ions. However, it probably helps to prevent ions that have entered the 6P from diffusing back upstream toward the IF.

rf Heating in the IF

Initial efforts involved a configuration where ions exited the ion funnel directly into the DIFF region without the 6P present, ESI/IF. Although this arrangement produces excellent intensities and reasonable kinetic energy distributions, using the IF without subsequent thermalization steps can result in ions picking up internal energy in excess of thermal temperatures, i.e., the internal energies of the ions are no longer well described by a Maxwell–Boltzmann distribution at room temperature. The internal energies may still be satisfactorily described using a higher temperature dis-

tribution, but this temperature is now either unknown or poorly defined and dependent on experimental conditions.

Figure 2 shows the CID cross section of the Na^+ loss from Na^+(proline) produced by the ESI/IF source described earlier at two different rf voltages applied to the IF, Vpp. For reference, CID results for the same system are shown with the ions generated using a DC/FT source. Clearly, the onset energy of the Na^+ shifts to lower energies as the IF Vpp increases. Such a shift in the threshold energy is an unambiguous symptom that the ions are being heated. In the case of the Na^+(proline), at a Vpp of 30 V, the system picks up roughly 1 eV of internal energy. Analysis of the Vpp = 20 and 30 V results are consistent with ions having a temperature of about 500 and 700 K, respectively. Given the scarcity of information in the literature regarding the temperature of ions produced by electrospray, it is reasonable to question the source of the internal energy increase. It is unknown whether the ions are heated exclusively by the IF or whether the ESI source also contributes.

Figure 3 shows Na^+(2-propanol) CID results for ions produced using the DC/FT source and therefore thermalized, before being introduced into the IF. For all cases, the IF was kept at a DC voltage drop of 4 V and an rf frequency of 1.5 MHz. Changes in the rf frequency over a range of 1–2 MHz or in the DC voltage drop across the funnel over a range of 4–20 V while holding the Vpp constant do not lead to changes in the internal energy of the ions. Figure 3 shows that there is little change in the threshold energy with Vpp values ranging from 5 to 14 V and, furthermore, the results correspond to thermalized ions [37]. However, at an IF Vpp of 25 V, the ions clearly begin picking up internal energy (~0.1 eV). The results in Figures 2 and 3 demonstrate that the ions are picking up excess energy in the ion funnel. Although the Na^+(2-propanol) does not pick up as much internal energy as the Na^+(proline) at similar Vpp values, this is most likely a function of the number and magnitude of vibrational modes available in each system. It is possible that thermal ions could be produced by systematically decreasing the IF Vpp until the measured threshold ceases to exhibit signs of heating. However, lowering Vpp greatly decreases the overall signal intensity, thus defeating the purpose of the IF!

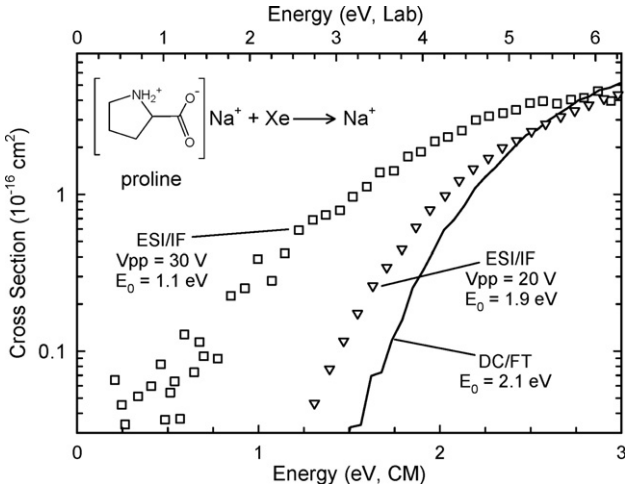

Figure 2. Cross sections for collision-induced dissociation of Na^+(proline) with Xe as a function of kinetic energy in the center-of-mass frame (lower *x*-axis) and the laboratory frame (upper *x*-axis). The solid line shows thermalized ions produced with a DC discharge/flow tube source. Open triangles (▽) and open squares (□) show data produced using an ESI source and ion funnel (ESI/IF) without the hexapole shown in Figure 1 with an IF rf Vpp of 20 and 30 V, respectively.

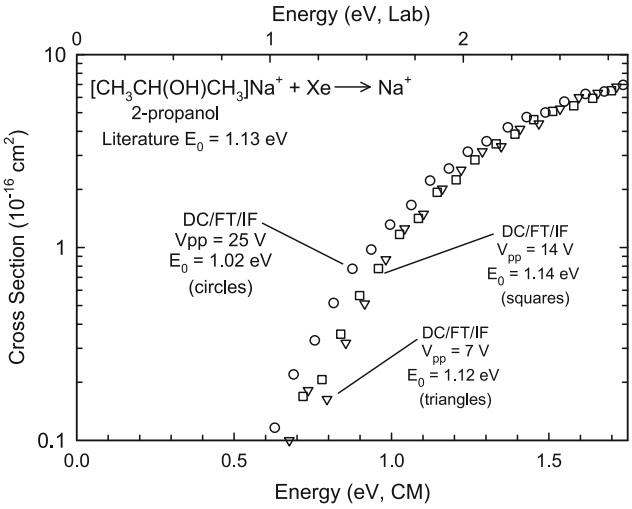

Figure 3. Cross sections for collision-induced dissociation of Na^+(2-propanol) with Xe as a function of kinetic energy in the center-of-mass frame (lower *x*-axis) and the laboratory frame (upper *x*-axis). All data were produced using a DC discharge/flow tube source and ion funnel (DC/FT/IF). Open triangles (▽) show results for the rf Vpp on the IF of 7 V. Open squares (□) and open circles (○) show Vpp = 14 and 25 V, respectively. Results at the lower Vpp values match the literature [36].

Hexapole Ion Guide

The hexapole ion guide (6P) consists of six 0.125-in. centerless ground stainless steel rods (Small Parts), 5.50 in. long, equally spaced on a 0.375-in. BC. Each rod has

0-80 tapped holes in two locations. The rods are held in place and centered using 0-80 screws inserted through a machined Torlon (a polyamide-imide thermoplastic) disc with "cups" cut out that encircle roughly 1/3 of the rod diameter. Electrical connections to the rods are also made using the 0-80 screws. The Torlon pieces attach to either end of the ligand exchange cell (LXC), which aligns the 6P with respect to the IF. Gases can be added to the LXC to react with ions produced by the ESI by ligand exchange or condensation. This has proven to be a useful feature for making ion complexes with ligands other than the solvent used in the electrospray process as well as creating larger ion/solvent clusters. The rf signal is applied to the rods using a simple rf generator described by Jones et al. [38, 39] and is normally operated at a frequency of 5.5 MHz with a peak to peak voltage (Vpp) of 200–300 V. The DC voltage of the 6P is maintained at 0 V, but can be adjusted.

One of the unique features of this 6P is that it spans two vacuum regions with the rods serving as the conductance limiting aperture. While running the ESI, pressures in the SRC region are approximately 20–40 mTorr and about 8×10^{-5} Torr in the DIFF region. The gas flow between the two regions is further limited by placing a 0.5-in.-long piece of machined Torlon with cups that encircle one half of each rod. The 6P rods extend about 2.0 in. into the higher vacuum region. The 6P must be located in the higher pressure region of the instrument to provide sufficient ion/neutral collisions for thermalization. We have tried placing the hexapole solely in the higher pressure source region of the instrument with a small lens to extract the ions into the differentially pumped region. This results in a moderate loss of intensity and kinetic energy distributions that are two- to fourfold broader relative to the configuration where the hexapole spans both regions.

We have tested experimental configurations lacking the IF by injecting ions directly from the heated capillary into the 6P, ESI/6P. This does result in signal intensities comparable to using the ion funnel, but the hexapole quickly becomes fouled by spray deposits. The most noticeable symptom of this residue is that there is a noticeable increase in the ion kinetic energy. With the ESI/6P, we have observed kinetic energies rising by 1–3 eV in as short a time as 3–4 h, roughly the timeframe to collect data at three to four different collision cell pressures. Under such conditions, thermalization of the ions is dubious and eventually the signal intensity for higher *m/z* ions begins to significantly attenuate. With the ion funnel and jet disrupter inserted before the 6P, kinetic energy distributions are stable for >10 days. From a practical perspective, this results in venting and cleaning of the hexapole on a much less frequent basis.

We have also tried placing a DC "extraction" lens on the exit side of the 6P where the lens inserts into the center of the 6P, similar in design to the TL at the IF/6P interface. However, use of such a lens leads to kinetic energy distributions broadened by a factor of about 3

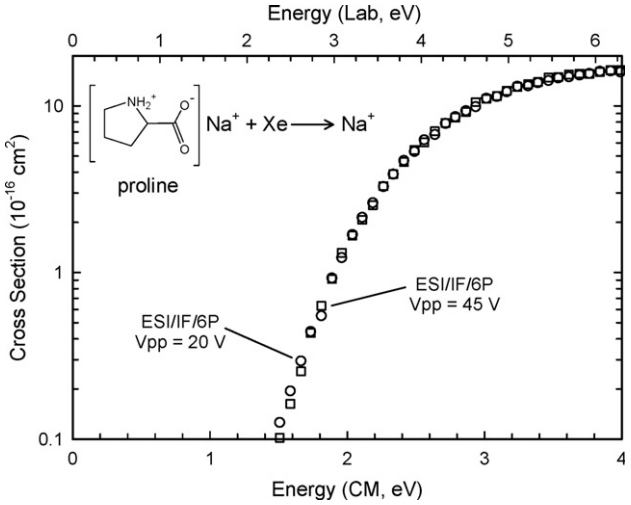

Figure 4. Cross sections for collision-induced dissociation of Na^+(proline) with Xe as a function of kinetic energy in the center-of-mass frame (lower *x*-axis) and the laboratory frame (upper *x*-axis). Open circles (○) and open squares (□) show data produced using the electrospray/ion funnel/hexapole (ESI/IF/6P) configuration as shown in Figure 1 using an rf Vpp on the IF of 20 and 45 V, respectively.

and slightly lower ion intensities. Currently, the first DC lens following the 6P is placed about 0.5 in. from the end of the 6P and has an ID of 0.375 in. and therefore minimally perturbs the ions exiting the 6P. The ion beam emanating from the 6P is well collimated compared to the more diffuse beam produced by our DC/FT source. As a result, the beam intensity can be greatly attenuated if the ESI/IF/6P is slightly misaligned relative to the electrostatic lenses located farther down the beam line. A set of DC deflectors placed about 1 in. from the exit of the 6P has proven to be of great benefit for correcting any minor alignment issues.

As with Figure 2, Figure 4 shows the CID cross section for Na^+ loss from Na^+(proline). However, in Figure 4 a 6P has been added to the ESI/IF configuration used in Figure 2 to reproduce the ESI/IF/6P experimental arrangement as shown in Figure 1. The cross sections in Figure 4 illustrate that with the addition of the 6P, the threshold energies are independent of Vpp in the IF. The thresholds measured for these ions are identical to those previously published for ions generated using the DC/FT source.

As mentioned previously, the pressures in the source region of the instrument generally range from 20 to 40 mTorr (when no gas is added to the LXC). At these pressures, the mean free path of the ions is <10 mm. Thus, regardless of the voltage drop between the IF and 6P, the ions quickly slow kinetically and begin to diffuse along the axis of the 6P. This leads to a high number of ion/neutral collisions in the 6P such that conditions in the ion funnel may be optimized for ion intensity without concern for conditions leading to non-thermal internal energy distributions. Conditions upstream from the IF, such as the temperature of the

capillary tubing (tested over a range from 60 to 150 °C), ESN voltage or syringe pump speed also have no impact on the thermalization of the ions.

The experimental observations in Figure 4 were verified by simulations of the IF/6P configuration using SIMION with a realistic ion/neutral collision model [40]. These simulations clearly show that the 6P is indeed a very efficient radial trap for ions. At pressures typically found in the source region, the ions are quickly focused to the middle of the rods by collisional cooling. Once the ions reach the center of the rods, they enter a nearly field-free region, which allows them to undergo thermalizing collisions with the neutral gas. However, it is imperative to appreciate that the hexapole provides no driving force for ions in the axial direction. This is in direct contrast to the ion funnel where the ions are pulled through by the DC voltage gradient. Placing the IF and 6P in series provides the opportunity to take advantage of each device while still meeting the stringent conditions necessary for an ion source used for TCID.

Results and Discussion

Ion Stabilities and Intensities

The intensity and stability of the ion beam is primarily a function of the electrospray conditions. Small changes in variables such as the solution concentration, selection of solvent, and flow rate may necessitate adjustment to the needle bias and its relative location to the entrance orifice to find optimal spray conditions.

Although the needle assembly can also be used with fused silica capillaries, 35-gauge stainless steel needles provide excellent intensity and stability for the complexes normally observed with the GIBMS. However, care must be observed when using such thin wall (0.0016-in.) tubing because small amounts of oxidation can result in the formation of minute holes. These openings can draw air into the electrospray solution within the needle, resulting in the spray flickering. The resulting instability in the ion intensity is unsuitable for TCID data collection.

Figure 5 shows a representative 120-min scan of the Na^+(proline) ion produced from a 10^{-4} M solution of NaCl and proline using the ESI/IF/6P. The average intensity over the duration of the scan is 6.0×10^5 ions/s with a standard deviation over this period of <5%. Both the intensity and stability of this beam are comparable to other sources used with the GIBMS.

Kinetic Energies

An example kinetic energy profile for the ESI/IF/6P source (Lab and CM) is shown in Figure 6a for $H_3O^+(H_2O)_2$ and Figure 6b for Na^+(proline). The derivative of the kinetic energy onset and its fit to a Gaussian distribution are also shown. For clarity, intensities have been normalized to unity, but the absolute intensity of both systems is approximately 1×10^6 ions/s.

Figure 6 clearly shows that the derivative of the kinetic energy onset is well described by a Gaussian fit. For the Na^+(proline) scan, the KE_0 is −0.39 eV with a FWHM of 0.16 eV. The $H_3O^+(H_2O)_2$ scan shows very similar results with a KE_0 of −0.38 eV and a FWHM of 0.14 eV. The FWHM of the kinetic energy distribution is typically 0.09–0.20 eV in the laboratory frame of reference using the ESI/IF/6P source. For comparison, the FWHM of a one-dimensional Boltzmann velocity distribution at 300 K is only 0.072 eV. Thus the distortions resulting from focusing aberrations, space charge effects, and other instrumental parameters are minimized for the ESI/IF/6P source.

The FWHM values for the ESI/IF/6P are also considerably smaller than the values cited by other groups using an ESI source for TCID. Andersen et al. [2] state FWHM values of 0.6 eV for $H_5O_2^+$ to 1.2 eV for $H_9O_4^+$ in the laboratory frame. In later work from the same group [4], the kinetic energy broadening was reduced (although not quantified), at a cost of a loss of ion intensity. Hinderling et al. [5] state values of 0.4–0.6 eV in the laboratory frame using an ESI source. Moreover, the kinetic energy distributions produced by the ESI/IF/6P source are narrower than those produced in the DC/FT, which has FWHM values typically 0.25–0.50 eV in the lab frame. Likely the narrow kinetic energy distributions in the ESI/IF/6P source because the ions traverse most of the length of the 6P by diffusion.

As mentioned previously, a number of experiments were performed to confirm that conditions within the ion funnel do not affect the resulting kinetic energy distributions. The kinetic energy distributions produced by the ESI/IF/6P source show no dependency on the ion mass over the range of m/z = 30–170 Da, on the Vpp of the 6P from 150 to 400 V,

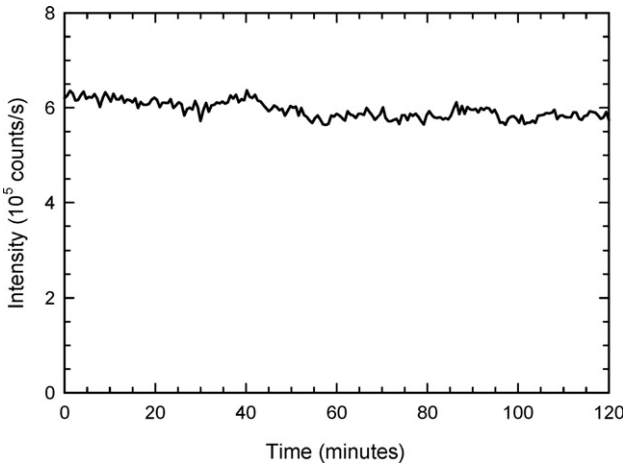

Figure 5. Stability profile of a parent ion beam produced by the ESI/IF/6P source. Scan is of 10^{-4} M spray of Na^+(proline) in a solvent of 50:50 water:methanol. Average intensity for duration of scan is $6.0 \pm 0.3 \times 10^5$ ions/s.

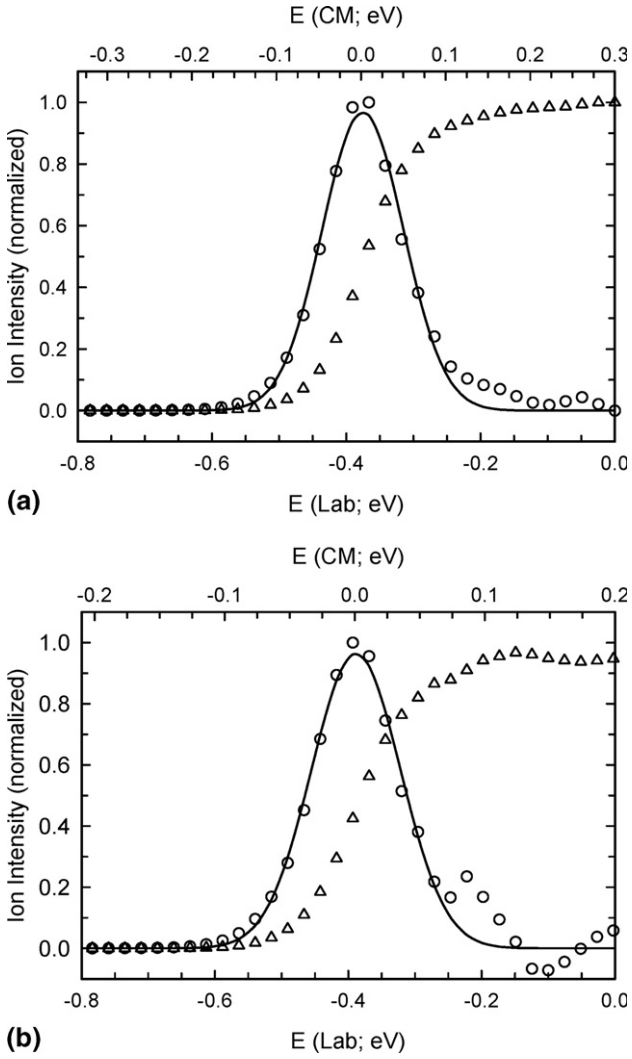

Figure 6. Kinetic energy profile for (**a**) $H_3O^+(H_2O)_2$ and (**b**) Na^+(proline), shown in the laboratory frame (lower *x*-axis) and center-of-mass frame (upper *x*-axis, assuming Xe collision gas). Open triangles (△) show the normalized ion intensity versus DC voltage on the octopole near the zero of energy. For both (**a**) and (**b**), the maximum ion intensity was about 1×10^6 ions/s. Open circles (○) are the first derivative of the ion intensity. Solid lines show the best fit to a Gaussian distribution. For (**a**) $E_0 = -0.375$ eV, FWHM = 0.143 eV (Lab); (**b**) $E_0 = -0.388$ eV, FWHM = 0.157 eV (Lab).

or on the rf frequency of the 6P from 4 to 6 MHz. In Figure 6, the voltage drop between the IF and 6P was 7 and 1 V for the Na^+(proline) and $H_3O^+(H_2O)_2$ systems, respectively; nevertheless the KE_0 in both cases remains at about 0.38 V. This reiterates that ions injected into the 5.5-in.-long 6P quickly undergo sufficient collisions to kinetically equilibrate. One advantage of such equilibration is that it allows for conditions in the IF to be adjusted to generate different ion distributions for analysis without concern that optimal conditions for production of the ions could lead to non-thermal internal energy distributions for analysis.

Thermalization

Figure 7a and b show example pressure extrapolated cross sections for $H_3O^+(H_2O)_2$ and Na^+(proline), respectively, produced using the ESI/IF/6P source. These figures also include the corresponding convoluted and unconvoluted fits to eq 1. The experimental cross sections are reproduced by eq 1 over a large range of collision energies (2–4 eV), over at least a factor of 100 in magnitude and within an absolute cross section of about 0.1×10^{-16} cm^2.

Table 1 shows TCID results for ions produced by the ESI/IF/6P source compared to a number of DC/FT studies performed by this lab for the Na^+(proline) [17] and $H_3O^+(H_2O)_x$ (x = 1–3) [15, 41] systems. All of the TCID results in the table include pressure extrapolations and RRKM corrections as described earlier. Table 1 also in-

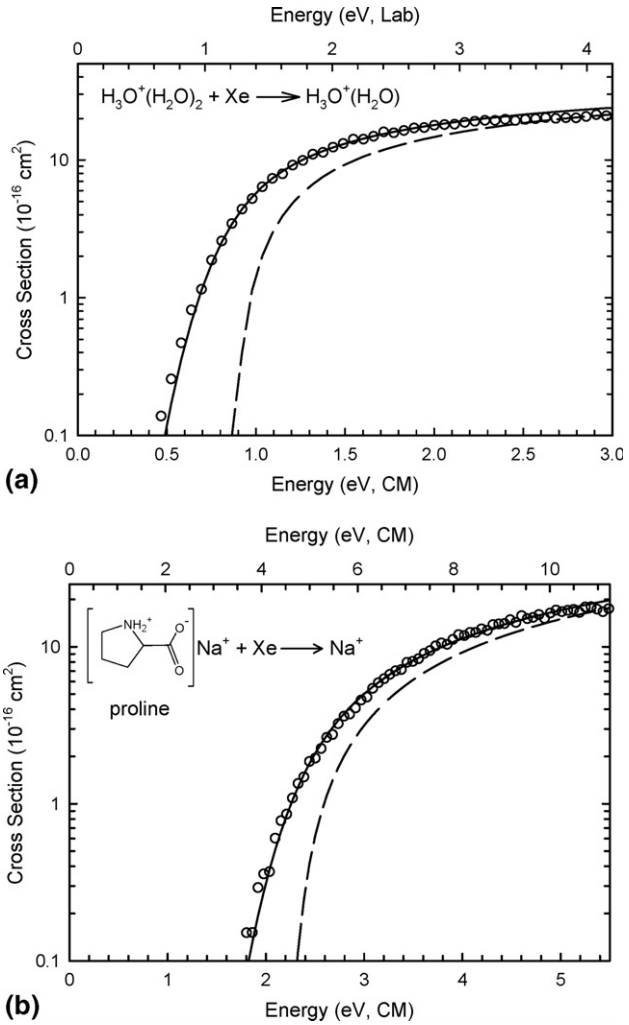

Figure 7. Zero-pressure extrapolated cross sections for collision-induced dissociation of (**a**) $H_3O^+(H_2O)_2$ and (**b**) Na^+(proline) with Xe in the threshold region as a function of kinetic energy in the center-of-mass frame (lower *x*-axis) and the laboratory frame (upper *x*-axis). Solid lines show the best fit to the data using the model of eq 1 convoluted over the neutral and ion kinetic and internal energy distributions. Dashed lines show the model cross sections in the absence of experimental kinetic energy broadening for reactions with an internal energy of 0 K.

Table 1. Comparison of ESI TCID results with fitting parameters for eq 1

System	Source	σ_0	n	E_0 (eV)	E_0, literature
Na^+(proline) → Na^+ + proline	ESI/IF/6P[a]	15.9 (1.0)	1.5 (0.1)	1.94 (0.08)	2.01 (0.08)[d]
	DC/FT[b]	15.4 (1.0)	1.4 (0.1)	1.93 (0.06)	1.80 (0.12)[e]
$H_5O_2^+$ → H_3O^+ + H_2O	ESI/IF/6P[a]	5.6 (0.4)	1.5 (0.2)	1.44 (0.06)	1.37 (0.04)[f] 1.65 (0.10)[g] 1.62 (0.08)[h]
	DC/FT[c]	4.0 (0.2)	1.5 (0.1)	1.40 (0.04)	1.4 (0.1)[i] 1.24 (0.09)[j]
$H_7O_3^+$ → $H_5O_2^+$ + H_2O	ESI/IF/6P[a]	25.8 (1.4)	1.2 (0.1)	0.88 (0.05)	0.85 (0.04)[f] 0.90 (0.10)[g]
	DC/FT[c]	18.6 (0.8)	1.5 (0.2)	0.89 (0.06)	0.96 (0.04)[h] 0.82 (0.04)[k]
$H_9O_4^+$ → $H_7O_3^+$ + H_2O	ESI/IF/6P[a]	37.9 (2.8)	1.0 (0.1)	0.72 (0.05)	0.72 (0.04)[g] 0.77 (0.05)[h]
	DC/FT[c]	38.6 (2.0)	1.2 (0.3)	0.73 (0.06)	0.69 (0.04)[k] 0.78 (0.04)[l]

ESI, electrospray ionization source; TCID, threshold collision-induced dissociation; DC/FT, DC discharge/flow tube source; HPMS, high-pressure mass spectrometry; KM, kinetic method; ICR EQ, ion cyclotron resonance equilibrium.
[a]This work.
[b]TCID, DC/FT [17].
[c]TCID, DC/FT [15].
[d]KM [41].
[e]ICR EQ [42].
[f]HPMS [43].
[g]TCID [44].
[h]TCID [45].
[i]ESI, TCID [2].
[j]ESI, TCID [5] (E_0 converted from 298 K value using standard thermodynamic formulas).
[k]HPMS [46].
[l]HPMS [47].

cludes threshold values produced using other sources and experimental methodologies [2,5,41–47]. For all of the systems shown in Table 1, the ESI/IF/6P results produced using the configuration shown in Figure 1 yield threshold energies well within stated experimental uncertainties of the previous results. There is particularly excellent agreement for the magnitude of the cross section (σ_0), shape of the cross section (n), and the threshold value (E_0) between the TCID results produced in this lab using the DC/FT and ESI/IF/6P sources. Threshold values produced by the ESI/IF/6P source show such agreement over a >1-eV range of threshold values (0.7–1.9 eV) and for systems with m/z values ranging from 37 to 138 Da.

As with the kinetic energy distributions, the source is surprisingly robust to changes in conditions. Adjustments to the 6P parameters over ranges varying from 200 to 400 Vpp and 4 to 6 MHz do not produce any observable changes to the extracted threshold energies. Similarly, conditions in the IF or desolvation temperature of the CTH have no impact on measured threshold values. It is believed that this is primarily a consequence that the pressure in the source chamber under operating conditions is sufficiently high (20–40 mTorr) that the ions undergo many collisions before they diffuse to the exit of the 6P. A rough calculation of the average number of collisions undergone by a Na^+(proline) ion diffusing from the entrance of the 6P to the next chamber is $>10^4$, more than enough to ensure thermalization.

Conclusions

The electrospray source described here meets all four requirements necessary for rigorous thermochemical analysis: high signal intensity, signal stability, well-defined kinetic energy distributions, and ions with internal energies described by a Maxwell–Boltzmann distribution at room temperature. The use of an ion funnel with a jet disrupter and hexapole ion guide in series takes advantage of the intrinsic properties of both devices to collect, transfer, and thermalize ions emerging from the electrospray. Using either device alone can lead to poorly defined ion characteristics. The source is also extremely robust to changes in experimental parameters. The addition of the ESI source to the GIBMS opens the door for thermochemical analysis of a wide range of new and interesting systems for study. For example, TCID results for the hydration energies of multiply charged ions such as $Ca(H_2O)_x^{2+}$ (x = 5–9) show good agreement with previous literature values and with theory [48], but preliminary results show that the hydration energies of the inner solvent shell (x = 2–4) can also be obtained [49]. The binding energies of alkali cations to cysteine [50], the acidic amino acids (aspartic acid and glutamic acid), and their amide derivatives (asparagine and glutamine) [51] have been measured using this source and show good agreement with theory. Extensions to metallized di- and tripep-

tides have also been achieved with good results [24, 29, 52].

Acknowledgments

This work was funded by National Science Foundation Grant CHE0451477. A portion of the research reported herein was performed under user proposal #2223 in the Environmental Molecular Sciences Laboratory (EMSL) located at Pacific Northwest National Laboratory (PNNL). RMM thanks Keqi Tang and Sang-Wong Lee for their generous advice. The assistance of the University of Utah Department of Chemistry machine shop (Dennis Romney and Jeff Welch) and electronics shop (Ron Jones) was invaluable in the development of this instrument.

References

1. Yamashita, M.; Fenn, J. B. Electrospray Ion Source. Another Variation on the Free-jet Theme. *J. Phys. Chem.* **1984,** *88,* 4451–4459.
2. Andersen, S. G.; Blades, A. T.; Klassen, J. S.; Kebarle, P. Determination of Ion–Ligand Bond Energies and Ion Fragmentation Energies of Electrospray-produced Ions by Collision-induced Dissociation Threshold Measurements. *Int. J. Mass Spectrom. Ion Process.* **1995,** *141,* 217–228.
3. Poutsma, J. C.; Seburg, R. A.; Leonard, J. C.; Sunderlin, L. S.; Hill, B. T.; Hu, J.; Squires, R. R. Combining Electrospray Ionization and the Flowing Afterglow Method. *Rapid Commun. Mass Spectrom.* **1997,** *11,* 487–493.
4. Klassen, J. S.; Anderson, S. G.; Blades, A. T.; Kebarle, P. Reaction Enthalpies for $M^+L = M^+ + L$, Where $M^+ = Na^+$ and K^+ and L = Acetamide, N-Methylacetamide, N,N-Dimethylacetamide, Glycine, and Glycylglycine, from Determinations of the Collision-induced Dissociation Thresholds. *J. Phys. Chem.* **1996,** *100,* 14218–14227.
5. Hinderling, C.; Feichtinger, D.; Plattner, D. A.; Chen, P. A Combined Gas-Phase, Solution-Phase and Computational Study of C–H Activation by Cationic Iridium(III) Complexes. *J. Am. Chem. Soc.* **1997,** *119,* 10793–10804.
6. Ho, Y.; Kebarle, P. Studies of the Dissociation Mechanisms of Deprotonated Mononucleotides by Energy Resolved Collision-induced Dissociation. Int. J. Mass Spectrom. Ion Process. 1997, 165/166, 433–455.
7. Crain, P. F. Electrospray Ionization Mass Spectrometry of Nucleic Acids and Their Constituents. In *Electrospray Ionization Mass Spectrometry: Fundamentals Instrumentation and Applications*, Cole, R. B., Ed.; John Wiley & Sons: New York, 1997; pp 421–457.
8. Loo, J. A.; Ogorzsalek Loo, R. R. Electrospray Ionization Mass Spectrometry of Peptides and Proteins. In *Electrospray Ionization Mass Spectrometry: Fundamentals Instrumentation and Applications*, Cole, R. B., Ed.; John Wiley & Sons: New York, 1997; pp 385–419.
9. Ohashi, Y. Electrospray Ionization Mass Spectrometry of Carbohydrates and Lipids. In *Electrospray Ionization Mass Spectrometry: Fundamentals Instrumentation and Applications*, Cole, R. B., Ed.; John Wiley & Sons: New York, 1997; pp 459–498.
10. Gatlin, C. L.; Turecek, F. Acidity Determiniation in Droplets Formed by Electrospraying Methanol–Water Solutions. *Anal. Chem.* **1994,** *66,* 712–718.
11. Van Berkel, G. J.; McLuckey, S. A.; Glish, G. L. Electrochemical Origin of Radical Cations Observed in Electrospray Ionization Mass Spectra. *Anal. Chem.* **1992,** *64,* 1586–1593.
12. Gatlin, C. L.; Turecek, F. Electrospray Ionization of Inorganic and Organometallic Complexes. In *Electrospray Ionization Mass Spectrometry: Fundamentals Instrumentation and Applications*, Cole, R. B., Ed.; John Wiley & Sons: New York, 1997; pp 527–570.
13. Sherman, C. L.; Brodbelt, J. S. An Equilibrium Partitioning Model for Predicting Response to Host–Guest Complexation in Electrospray Ionization Mass Spectrometry. *Anal. Chem.* **2003,** *75,* 1828–1836.
14. Kempen, E. C.; Brodbelt, J. S.; Bartsch, R. A.; Jang, Y.; Kim, J. S. Investigation of Alkali Metal Cation Selectivities of Lariat Ethers by Electrospray Ionization Mass Spectrometry. *Anal. Chem.* **1999,** *71,* 5493–5550.
15. Dalleska, N. F.; Honma, K.; Armentrout, P. B. Stepwise Solvation Enthalpies of Protonated Water Clusters: Collision Induced Dissociation as an Alternative to Equilibrium Studies. *J. Am. Chem. Soc.* **1993,** *115,* 12125–12131.
16. Moision, R. M.; Armentrout, P. B. An Experimental and Theoretical Dissection of Sodium Cation/Glycine Interactions. *J. Phys. Chem. A* **2002,** *106,* 10350–10362.
17. Moision, R. M.; Armentrout, P. B. The Special Five-Membered Ring of Proline: An Experimental and Theoretical Investigation of Alkali Metal Cation Interactions with Proline and Its Four- and Six-Membered Ring Analogues. *J. Am. Chem. Soc.* **2006,** *110,* 3933–3946.
18. Amicangelo, J. C.; Armentrout, P. B. Absolute Binding Energies of Alkali-Metal Cations with Benzene Determined by Threshold Collision-induced Dissociation Experiments and Ab Initio Theory. *J. Phys. Chem. A* **2000,** *104,* 11420–11432.
19. Schultz, R. H.; Armentrout, P. B. Reactions of N_4^+ with Rare Gases from Thermal to 10 eV c.m.: Collision-induced Dissociation, Charge Transfer, and Ligand Exchange. *Int. J. Mass Spectrom. Ion Process.* **1991,** *107,* 29–48.
20. Muntean, F.; Armentrout, P. B. Guided Ion Beam Study of Collision-induced Dissociation Dynamics: Integral and Differential Cross Sections. *J. Chem. Phys.* **2001,** *115,* 1213–1228.
21. Ervin, K. M.; Armentrout, P. B. Translational Energy Dependence of $Ar^+ + XY \rightarrow ArX^+ + Y$ (XY = H_2, D_2, HD) from Thermal to 30 eV c.m. *J. Chem. Phys.* **1985,** *83,* 166–189.
22. Teloy, E.; Gerlich, D. Integral Cross Sections for Ion–Molecule Reactions. 1. The Guided Beam Technique. *Chem. Phys.* **1974,** *4,* 417–427.
23. Gerlich, D. Inhomogeneous rf Fields: A Versatile Tool for the Study of Processes with Slow Ions. *Adv. Chem. Phys.* **1992,** *82,* 1–176.
24. Schultz, R. H.; Armentrout, P. B. Threshold Collisional Activation of $FeC_2H_6^+$: $Fe^+ \cdot$ ethane vs. $Fe^+ \cdot$ dimethyl Structures. *J. Phys. Chem.* **1992,** *96,* 1662–1667.
25. Rodgers, M. T. Substituent Effects in the Binding of Alkali Metal Ions to Pyridines Studied by Threshold Collision-induced Dissociation and Ab Initio Theory: The Aminopyridines. *J. Phys. Chem. A* **2001,** *105,* 8145–8153.
26. Rodgers, M. T.; Armentrout, P. B. An Absolute Sodium Cation Affinity Scale: Threshold Collision-induced Dissociation Experiments and Ab Initio Theory. *J. Phys. Chem. A* **2000,** *104,* 2238–2247.
27. Amunugama, R.; Rodgers, M. T. The Influence of Substituents on Cation–π Interactions. 1. Absolute Binding Energies of Alkali Metal Cation–Toluene Complexes Determined by Threshold Collision-induced Dissociation and Theoretical Studies. *J. Phys. Chem. A* **2002,** *106,* 5529–5539.
28. Armentrout, P. B. Thermochemical Measurements by Guided Ion Beam Mass Spectrometry. In *Advances in Gas Phase Ion Chemistry*, Adams, N. G.; Babcock, L. M., Eds.; JAI Press: Greenwich, CT, 1992; Vol. 1, pp 83–119.
29. Chantry, P. J. Doppler Broadening in Beam Experiments. *J. Chem. Phys.* **1971,** *55,* 2746–2759.
30. Lifshitz, C.; Wu, R. L. C.; Tiernan, T. O.; Terwilliger, D. T. Negative Ion–Molecule Reactions of Ozone and Their Implications on the Thermochemistry of O_3^-. *J. Chem. Phys.* **1978,** *68,* 247–260.
31. Rodgers, M. T.; Ervin, K. M.; Armentrout, P. B. Statistical Modeling of Collision-induced Dissociation Thresholds. *J. Chem. Phys.* **1997,** *106,* 4499–4508.
32. Shaffer, S. A.; Prior, D. C.; Anderson, G. A.; Udseth, H. R.; Smith, R. D. An Ion Funnel Interface for Improved Ion Focusing and Sensitivity Using Electrospray Ionization Mass Spectrometry. *Anal. Chem.* **1998,** *70,* 4111–4119.
33. Shaffer, S. A.; Tolmachev, A.; Prior, D. C.; Anderson, G. A.; Udseth, H. R.; Smith, R. D. Characterization of an Improved Electrodynamic Ion Funnel Interface for Electrospray Ionization Mass Spectrometry. *Anal. Chem.* **1999,** *71,* 2957–2964.
34. Belov, M. E.; Gorshkov, M. V.; Udseth, H. R.; Anderson, G. A.; Smith, R. D. Zeptomole-Sensitivity Electrospray Ionization–Fourier Transform Ion Cyclotron Resonance Mass Spectrometry of Proteins. *Anal. Chem.* **2000,** *72,* 2271–2279.
35. Kim, T.; Udseth, H. R.; Smith, R. D. A Multicapillary Inlet Jet Disruption Electrodynamic Ion Funnel Interface for Improved Sensitivity Using Atmospheric Pressure Ion Sources. *Anal. Chem.* **2001,** *73,* 4162–4170.
36. Tang, K.; Tolmachev, A.; Nikolaev, E.; Zhang, R.; Belov, M. E.; Udseth, H. R.; Smith, R. D. Independent Control of Ion Transmission in a Jet Disrupter Dual-Channel Ion Funnel Electrospray Ionization MS Interface. *Anal. Chem.* **2002,** *74,* 5431–5437.
37. Rodgers, M. T.; Armentrout, P. B. Absolute Binding Energies of Sodium Ions to Short Chain Alcohols Determined by Threshold Collision-induced Dissociation Experiments and Ab Initio Theory. *J. Phys. Chem. A* **1999,** *103,* 4955–4963.
38. Jones, R. M.; Anderson, S. L. Simplified Radio-Frequency Generator for Driving Ion Guides, Traps and Other Capacitive Loads. *Rev. Sci. Instrum.* **2000,** *71,* 4335–4337.
39. Jones, R. M.; Gerlich, D.; Anderson, S. L. Simple Radio-Frequency Power Source for Ion Guides and Ion Traps. *Rev. Sci. Instrum.* **1997,** *68,* 3357–3362.
40. Manura,, D. *A Hard-Sphere, Elastic, Ion-Neutral Collision Model for SIMION*. Available at collision_hs1.prg rev. 2-2005-07-13. Scientific Instrument Services, Inc., Ringoes, NJ: 2006.
41. Kish, M. M.; Ohanessian, G.; Wesdemiotis, C. The Na^+ Affinities of α-Amino Acids: Side-chain Substituent Effects. *Int. J. Mass Spectrom.* **2003,** *227,* 509–524.
42. Gapeev, A.; Dunbar, R. C. Na^+ Affinities of Gas-phase Amino Acids by Ligand Exchange Equilibrium. *Int. J. Mass Spectrom.* **2003,** *228,* 825–839.
43. Cunningham, A. J.; Payzant, A. D.; Kebarle, P. Kinetic Study of the Proton Hydrate $H^+(H_2O)_n$ Equilibriums in the Gas Phase. *J. Am. Chem. Soc.* **1972,** *94,* 7627–7632.
44. Honma, K.; Sunderlin, L. S.; Armentrout, P. B. Reactions of Protonated Water Clusters with Deuterated Ammonia $H(H_2O)_n^+$ (n = 1–4) + ND_3. *Int. J. Mass Spectrom. Ion Process.* **1992,** *117,* 237–259.
45. Honma, K.; Sunderlin, L. S.; Armentrout, P. B. Guided-ion Beam Studies of the Reactions of Protonated Water Clusters, $H(H_2O)_n^+$ (n = 1–4). *J. Chem. Phys.* **1993,** *99,* 1623–1632.
46. Meot-Ner, M.; Speller, C. V. Filling Solvent Shells about Ions. 1. Thermochemical Criteria and the Effects of Isomeric Clusters. *J. Phys. Chem.* **1986,** *90,* 6616–6624.

47. Lau, Y. K.; Ikuta, S.; Kebarle, P. Thermodynamics and Kinetics of the Gas-phase Reactions $H_3O^+(H_2O)_{n-1}$ + Water = $H_3O^+(H_2O)_n$. *J. Am. Chem. Soc.* **1982,** *104,* 1462–1469.
48. Carl, D.; Moision, R. M.; Armentrout, P. B. Binding Energies for the Inner Hydration Shells of Ca^{2+}: An Experimental and Theoretical Investigation of $Ca^{2+}(H_2O)_x$ Complexes (x = 5–9). *Int. J. Mass Spectrom.*, accepted for publication.
49. Carl, D.; Moision, R. M.; Armentrout, P. B. Binding Energies for the Innermost Hydration Shell of Ca^{2+}: An Experimental and Theoretical Investigation of $Ca^{2+}(H_2O)_x$ Complexes (x = 1–4). Work in progress.
50. Ye, S. J.; Moision, R. M.; Armentrout, P. B. Alkali Cation Binding Energies to Cysteine: Threshold Collision-induced Dissociation and Theoretical Studies. Work in progress.
51. Heaton, A. L.; Moision, R. M.; Armentrout, P. B. Binding Energies of the Alkali Cations to the Acidic Amino Acids (Asp, Glu), Their Amide Derivatives (Asn, Gln), and Their Dehydration/Deamidation Fragments: Theory and Experiment. Work in progress.
52. Ye, S. J.; Moision, R. M.; Armentrout, P. B. Threshold Collision Induced Dissociation Studies of the Binding Energies of Alkali Cations to Small Peptides: Gly-Gly and Gly-Gly-Gly. Work in progress.